Double-wavelet Double-difference elastic full-waveform inversion

Xin Fu, Scott Keating, Kris Innanen and Qi Hu

ABSTRACT

Full-wave inversion (FWI) based on the wave equation has been employed extensively in geophysics. Time-lapse FWI that can detect time-lapse property changes of the subsurface with a high resolution has become an important tool. As a popular inversion time-lapse strategy, double-difference FWI (DDFWI) contains twice inversions, the first inversion is the baseline inversion, in which the input elements are the baseline data and a reasonable initial model, in the second monitoring inversion, DDFWI uses the starting model of the inverted baseline model and a composited data as an alternative of the monitoring data, that is, the difference data (the difference between the monitoring data and the baseline data) plus the synthetic data of the inverted baseline model. Since DDFWI is using the difference data, which helps it to focus on the target time-lapse area, thus DDFWI has fewer coherent errors in the inverted time-lapse model. But DDFWI also is of the shortcoming of requiring good repeatability of baseline and monitoring surveys, especially, when the wavelets of baseline data and monitoring data are different, the coherent errors are very heavy. To solve this problem, Fu et al. (2020) have developed a double-wavelet DDFWI method and implemented for the acoustic FWI. In this study, we will expand the double-wavelet method to the elastic FWI.

INTRODUCTION

Full-wave inversion (FWI) (Lailly et al., 1983; Tarantola, 1984; Virieux and Operto, 2009) based on the wave equation has been employed extensively in geophysics. Time-lapse FWI that can detect time-lapse property changes of the subsurface with a high resolution has become an important tool. Conducting time-lapse FWI normally contains twice inversions, a baseline inversion for the baseline model and a monitoring inversion for the monitoring model, and the time-lapse model is produced by subtracting the baseline model from the monitoring model. Only consider how data and starting models are used, inversion strategies of the time-lapse FWI can be classified into three basic categories, including the parallel difference FWI (using baseline data and monitoring data independently, using the same starting model for twice inversions), the sequential difference FWI (using baseline data and monitoring data independently, using the inverted baseline model for monitoring inversion) (Oldenborger et al., 2007; Routh and Anno, 2008), and the double-difference FWI (DDFWI) (Watanabe et al., 2004; Onishi et al., 2009; Denli and Huang, 2009; Zheng et al., 2011; Asnaashari et al., 2011; Routh et al., 2012; Raknes et al., 2013; Maharramov and Biondi, 2014; Raknes and Arntsen, 2014; Yang et al., 2016) adopted in this work.

In DDFWI, the first inversion is the baseline inversion that is the same as the other strategies, in which the input elements are the baseline data and a reasonable starting model. But in the second monitoring inversion, DDFWI uses a composited data as an alternative of the monitoring data, which is the difference data (the difference between the monitoring data and the baseline data) plus the synthetic data of the inverted baseline model. Since

FWI is extremely easy to be trapped into a local minimum, it means the twice inversions in both the parallel difference FWI and sequential difference FWI will yield different convergences on inverted models, it causes coherent errors on the final inverted time-lapse model (Asnaashari et al., 2014; Yang et al., 2015). Nevertheless, DDFWI is using the difference data, which helps it to focus on the target time-lapse area, thus DDFWI has fewer coherent errors in the inverted time-lapse model. Although DDFWI also is of the shortcoming of requiring good repeatability of baseline and monitoring surveys (Yang et al., 2015), with the efforts of researchers, some demerits have been improved, for instance, Hicks (2002) and Yang et al. (2016) use the interpolation technique to resample baseline and monitoring data to the same grids, Fu et al. (2020) develop a double-wavelet DDFWI method for acoustic FWI to solve the case that the wavelets of baseline data and monitoring data are different. In this study, we will expand the double-wavelet method to elastic FWI (EFWI).

THEORY

Elastic full-waveform inversion

EFWI starts from a given model $\mathbf{m}_0$ and uses an optimization method to search a model $\mathbf{m}$ that makes the synthetic data $\mathbf{d}_{syn}(\mathbf{m})$ match the observed data $\mathbf{d}_{obs}$ best. Usually, this is achieved by minimizing the L2 norm of data residual $\Delta\mathbf{d}$ $(\mathbf{d}_{syn}(\mathbf{m}) - \mathbf{d}_{obs})$ given by

$$E(\mathbf{m}) = \frac{1}{2}\Delta\mathbf{d}^T\Delta\mathbf{d}^*, \tag{1}$$

where T denotes the transpose of a matrix and $*$ denotes the complex conjugate. For EFWI, the model $\mathbf{m}$ in equation 1 represents the elastic parameters (e.g. P-wave velocity, S-wave velocity, and density), and $\mathbf{d}_{syn}$ is the wave field at receiver positions. In this paper, the wave field is obtained by soveling a frequency-domain 2D elastic wave equation given by

$$\begin{aligned}
&\omega^2\rho u + \frac{\partial}{\partial x}\left[(\lambda+2\mu)\frac{\partial u}{\partial x} + \lambda\frac{\partial v}{\partial z}\right] + \frac{\partial}{\partial z}\left[\mu\left(\frac{\partial u}{\partial z} + \frac{\partial v}{\partial x}\right)\right] + f = 0,\\
&\omega^2\rho v + \frac{\partial}{\partial z}\left[(\lambda+2\mu)\frac{\partial v}{\partial z} + \lambda\frac{\partial u}{\partial x}\right] + \frac{\partial}{\partial x}\left[\mu\left(\frac{\partial u}{\partial z} + \frac{\partial v}{\partial x}\right)\right] + g = 0,\\
&\mu = \rho {V_s}^2,\\
&\lambda = {V_p}^2\rho - 2\mu,
\end{aligned} \tag{2}$$

where ω is the angular frequency; $u = u(x, z, \omega)$, $v = v(x, z, \omega)$, $f = f(x, z, \omega)$, and $g = g(x, z, \omega)$ are, respectively, the horizontal displacement field, the vertical displacement field, the horizontal component of source, and the vertical component of source, all depend on the position (x, z) and ω; λ and μ are Lamé constants; $V_p = V_p(x, z)$, $V_s = V_s(x, z)$, and $\rho = \rho(x, z)$ are, respectively, P-wave velocity, S-wave velocity, and density, all depend on the position. Equation 2 can be discretized and solved by the finite-difference method (Pratt, 1990) under which it can be formulated as

$$\mathbf{A}\mathbf{u} = \mathbf{s}, \tag{3}$$

where $\mathbf{A}$ is the impedance matrix, $\mathbf{u} = [u, v]^T$ is the displacement vector, and $\mathbf{s} = [f, g]^T$ is the source vector.

The gradient of $E(\mathbf{m})$ in equation 1 with respect to $\mathbf{m}$ can be expressed as

$$\bigtriangledown_{\mathbf{m}} E = -\Re \left\{ \left[\frac{\partial \mathbf{u}}{\partial \mathbf{m}} \right]^T \Delta \mathbf{d}^* \right\}, \tag{4}$$

where $\Re$ denotes the real part operator. Differentiating equation 3 with respect to $\mathbf{m}$ gives

$$\mathbf{A} \frac{\partial \mathbf{u}}{\partial \mathbf{m}} = -\frac{\partial \mathbf{A}}{\partial \mathbf{m}} \mathbf{u}, \tag{5}$$

which tells us that the partial derivative wavefield $\partial \mathbf{u}/\partial \mathbf{m}$ can be calculated by solving the wave equation with a virtual source $-\left(\partial \mathbf{A}/\partial \mathbf{m}\right) \mathbf{u}$. Putting equation 5 into equation 4, we have

$$\bigtriangledown_{\mathbf{m}} E = \Re \left\{ \mathbf{u}^T \left[\frac{\partial \mathbf{A}}{\partial \mathbf{m}} \right] \mathbf{A}^{-1} \Delta \mathbf{d}^* \right\}, \tag{6}$$

from which, we can see that the adjoint wavefield $\mathbf{A}^{-1} \Delta \mathbf{d}^*$ is obtained by solving the wave equation with the source of the conjugate data residual. $\partial \mathbf{A}/\partial \mathbf{m}$ is referred to the radiation that can be used to investigate the crosstalk situation between different parameters (Brossier et al., 2009).

By minimizing the second-order Taylor expansion of the objective function, we can obtain the equation satisfied by the update of the Newton method, which is given by

$$\mathbf{H} \delta \mathbf{m} = - \bigtriangledown_{\mathbf{m}} E, \tag{7}$$

where $\mathbf{H}$ is the Hessian matrix, the second-order derivative of the misfit $E(\mathbf{m})$ with respect to $\mathbf{m}$. The Hessian matrix can compensate for the sphere spreading energy loss and mitigate the parameter crosstalk. However, the explicit Hessian and its inverse matrix consume huge computation and computer memory, it is unrealistic to find the exact Newton update in large-scale FWI. The truncated Gauss-Newton optimization method can overcome this difficulty. It uses a linear optimization method (the L-BFGS method in this work) to solve equation 7 to obtain a relatively accurate approximate Newton update, and the linear optimation method as a whole only needs to use the product of Hessian matrix and a known vector. After using the truncated Gauss-Newton optimation method, the updated model $\mathbf{m}$ is given by

$$\mathbf{m} = \mathbf{m} + \alpha \delta \mathbf{m}, \tag{8}$$

where α is the step length.

Double-difference time-lapse FWI

Thus in this study, we use the DDFWI that can focus on the time-lapse target and reduce coherent errors. In DDFWI, the first inversion is a baseline inversion for the baseline model, in which the input elements are the baseline data and a reasonable starting model. And in the second monitoring inversion for the monitoring model, DDFWI uses the inverted baseline model as the starting model and a composited data as an alternative to the monitoring data. The composited data is given by

$$\mathbf{d}'_{obs2} = \mathbf{b}_{syn}(\mathbf{m}'_1) + (\mathbf{d}_{obs2} - \mathbf{d}_{obs1}), \tag{9}$$

where $\mathbf{d}_{syn}(\mathbf{m}_1')$ is synthetic data of the inverted baseline model $\mathbf{m}_1'$, $\mathbf{d}_{obs2}$ and $\mathbf{d}_{obs1}$ are observed monitoring data and baseline data, respectively. Then during the monitoring inversion, the misfit function of DDFWI can be expressed as

$$E_{DDFWI}(\delta\mathbf{m}') = \frac{1}{2}||\mathbf{d}_{syn}(\mathbf{m}_1' + \delta\mathbf{m}') - \mathbf{d}_{obs2}'||^2, \tag{10}$$

where $||\ ||^2$ denots L2 norm, $\delta\mathbf{m}'$ is the model perturbation under the background model $\mathbf{m}_1'$. Defining

$$\delta\mathbf{d}_{syn}(\delta\mathbf{m}') = \mathbf{d}_{syn}(\mathbf{m}_1' + \delta\mathbf{m}') - \mathbf{d}_{syn}(\mathbf{m}_1'), \tag{11}$$

then

$$\mathbf{d}_{syn}(\mathbf{m}_1' + \delta\mathbf{m}') = \delta\mathbf{d}_{syn}(\delta\mathbf{m}') + \mathbf{d}_{syn}(\mathbf{m}_1'), \tag{12}$$

where $\delta\mathbf{d}_{syn}(\delta\mathbf{m}')$ is the synthetic difference data. Putting equation 9 and 12 into equation 10, we have

$$E_{DDFWI}(\delta\mathbf{m}') = \frac{1}{2}||\delta\mathbf{d}_{syn}(\delta\mathbf{m}') - \delta\mathbf{d}||^2, \tag{13}$$

where $\delta\mathbf{d} = \mathbf{d}_{obs2} - \mathbf{d}_{obs1}$ is the observed difference data. Therefore, when we are minimizing equation 10, actually, we are minimizing the residual of two difference data, that makes DDFWI focus on the target area. And finally, the inverted time-lapse model is $\delta\mathbf{m}'$.

But we have to note that the inverted time-lapse model $\delta\mathbf{m}'$ is different from the true time-lapse model $\delta\mathbf{m}$. $\delta\mathbf{m}'$ corresponds to the difference wavefield $\delta\mathbf{d}_{syn}(\delta\mathbf{m}')$ under the background wavefield $\mathbf{d}_{syn}(\mathbf{m}_1')$, but $\delta\mathbf{m}$ corresponds to the difference wavefield $\delta\mathbf{d}$ under the background wavefield $\mathbf{d}_{obs1}$. When $\mathbf{d}_{syn}(\mathbf{m}_1')$ is close to $\mathbf{d}_{obs1}$, i.e., $\mathbf{m}'$ is close to the true baseline model, $\delta\mathbf{m}'$ will be close to $\delta\mathbf{m}$, and vice versa. Thus a good inverted baseline model is important for DDFWI (Asnaashari et al., 2011).

Double-wavelet double-difference time-lapse waveform inversion

The reason why high repeatability is requested is that DDFWI needs the difference between monitor and baseline data sets to generate the composed data. When the perfect repeatability is reached, the data difference only contains the seismic response related to the change of underground parameters, which enables DDFWI to focus on the target. Nevertheless, when the wavelets of baseline and monitor data are different, the difference between the two data sets will come from both the wavelet contrast and the subsurface change. Generally, the subsurface change is weak, the little difference between the wavelets can easily submerge the effective information and cause heavy artifacts in the final inverted time-lapse model (Yang et al., 2015). We will also display this phenomenon in the numerical example section. For the case of the wavelets for the two data sets are different, Fu et al. (2020) has developed a double-wavelet double-difference time-lapse waveform inversion (DWDDFWI) and implemented to the acoustic FWI. To eliminate the data difference caused by the wavelet difference, DWDDFWI introduced below constructs a common wavelet for the baseline and monitor data.

To intuitively show how the subsurface parameter change influences the data set, we use Green's function to express the composited data in equation 9. A seismic data can

be expressed as the convolution between the source wavelet and Green's function, then equation 9 can be rewritten as

$$\mathbf{d}^{'}_{obs2} = \mathbf{d}_{syn}(\mathbf{m}^{'}_{1}) + (\mathbf{W}_{obs2} * \mathbf{G}_{obs2} - \mathbf{W}_{obs1} * \mathbf{G}_{obs1}), \tag{14}$$

where $*$ indicates the convolution operator; $\mathbf{W}_{obs2}$ and $\mathbf{W}_{obs1}$ are the source wavelets for monitor and baseline observed data, respectively; $\mathbf{G}_{obs2}$ and $\mathbf{G}_{obs1}$ are Green's functions for monitor and baseline observed data, respectively; and $\mathbf{d}_{syn}(\mathbf{m}^{'}_{1})$ is synthetic data using the baseline source wavelet $\mathbf{W}_{obs1}$. When $\mathbf{W}_{monitor}$ and $\mathbf{W}_{baseline}$ are identical, the difference is only from $\mathbf{G}_{obs2} - \mathbf{G}_{obs1}$ which is irrelevant to the wavelets. But in the case that $\mathbf{W}_{obs2}$ and $\mathbf{W}_{obs1}$ are not identical, the difference is from $\mathbf{W}_{obs2} * \mathbf{G}_{obs2} - \mathbf{W}_{obs1} * \mathbf{G}_{obs1}$ which is relevant both to the wavelets and Green's functions representing the property of the subsurface.

For the case of baseline and monitor wavelets are different, we reconstruct monitor data by performing the convolution between baseline wavelet and monitor data, and reconstruct monitor data by performing the convolution between monitor wavelet and baseline data, then the new composited data becomes:

$$\begin{aligned} \mathbf{d}^{''}_{obs2} &= \mathbf{d}^{'}_{syn}(\mathbf{m}^{'}_{1}) + (\mathbf{d}'_{obs2} - \mathbf{d}'_{obs1}) \\ &= \mathbf{d}^{'}_{syn}(\mathbf{m}^{'}_{1}) + (\mathbf{W}_{obs1} * \mathbf{d}_{obs2} - \mathbf{W}_{obs2} * \mathbf{d}_{obs1}), \end{aligned} \tag{15}$$

where $\mathbf{d}'_{obs2} = \mathbf{W}_{obs1} * \mathbf{d}_{obs2}$ and $\mathbf{d}'_{obs1} = \mathbf{W}_{obs2} * \mathbf{d}_{obs1}$ are the new observed monitoring data and new baseline data, respectively. Equation 15 can be expressed with Green's function as:

$$\begin{aligned} \mathbf{d}^{''}_{obs2} &= \mathbf{d}^{'}_{syn}(\mathbf{m}^{'}_{1}) + (\mathbf{W}_{obs1} * \mathbf{W}_{obs2} * \mathbf{G}_{obs2} - \mathbf{W}_{obs2} * \mathbf{W}_{obs1} * \mathbf{G}_{obs1}) \\ &= \mathbf{d}^{'}_{syn}(\mathbf{m}^{'}_{1}) + (\mathbf{W} * \mathbf{G}_{obs2} - \mathbf{W} * \mathbf{G}_{obs1}), \end{aligned} \tag{16}$$

where $\mathbf{W} = \mathbf{W}_{obs1} * \mathbf{W}_{obs2} = \mathbf{W}_{obs2} * \mathbf{W}_{obs1}$ is the double wavelet which used to forward modeling data $\mathbf{d}^{'}_{syn}(\mathbf{m}^{'}_{1})$ during the iterative wave inversion. After performing the reconstructions to baseline and monitor data sets, the new data sets are of the same wavelet $\mathbf{W}$, the data difference is from $\mathbf{G}_{obs2} - \mathbf{G}_{obs1}$ related to the subsurface change only.

NUMERICAL EXAMPLES

To demonstrate the feasibility of the DDFWI method for EFWI, we show some numerical examples using 2D elastic models in this section. The models and acquisition geometry are displayed in Figure1a-f. The model size is 50-by-50, model spacing is 10m, constant time-lapse changes are centered in the time-lapse models (the monitoring models minus the baseline models), 10 sources are spread on the surface, receivers are put on the surface, and two sides. Figure 2 displays the initial baseline models and inverted baseline models that are the starting models for the monitoring inversions in both DDFWI and DWDDFWI. Figure 3a-c display the inverted time-lapse models of DDFWI in the case of identical baseline wavelet (an 8Hz Ricker wavelet) and monitoring wavelet (an 8Hz Ricker wavelet). Figure 3d-e display the inverted time-lapse models of DDFWI in the case of different baseline wavelet (an 8Hz Ricker wavelet) and monitoring wavelet (a 10Hz Ricker wavelet). Figure

3f-i display the inverted time-lapse models of DWDDFWI in the case of different baseline wavelet (an 8Hz Ricker wavelet) and monitoring wavelet (a 10Hz Ricker wavelet). It shows that the difference between the wavelets impacts the inverted model heavily, and the DWDDFWI method for EFWI in the case of the baseline and monitoring data wavelets are different can provide the results as good as that provided by DDFWI in the case of the baseline and monitoring data wavelets are identical.

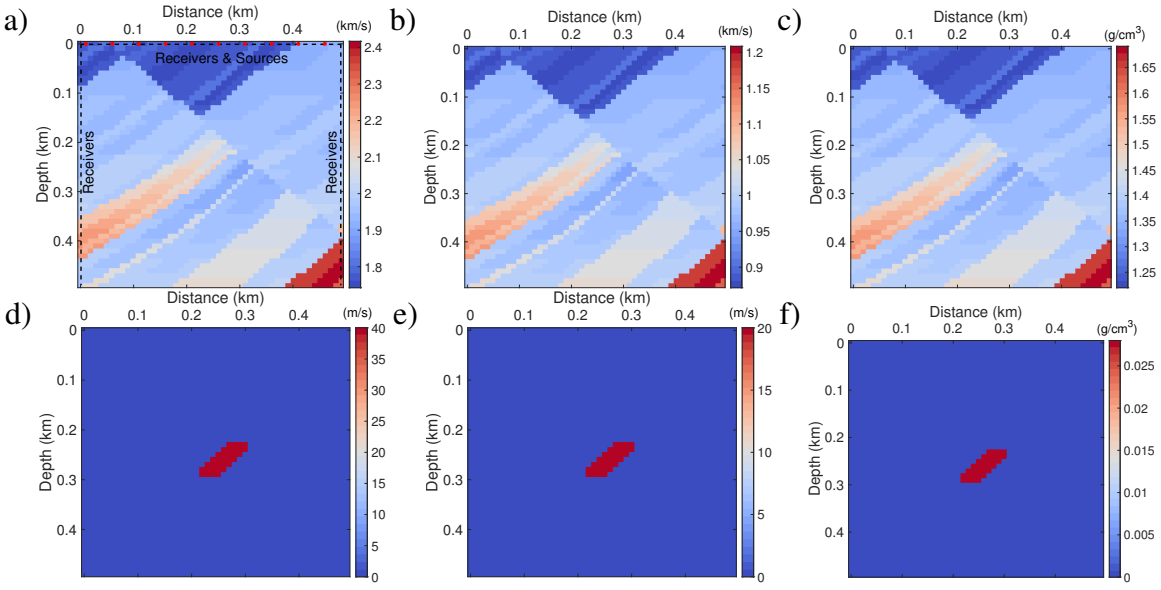

FIG. 1. True models and acquisition geometry.The true baseline models, (a) P-wave velocity, (b) S-wave velocity, and (c) density. The true time-lapse models, (d) P-wave velocity, (e) S-wave velocity, and (f) density.

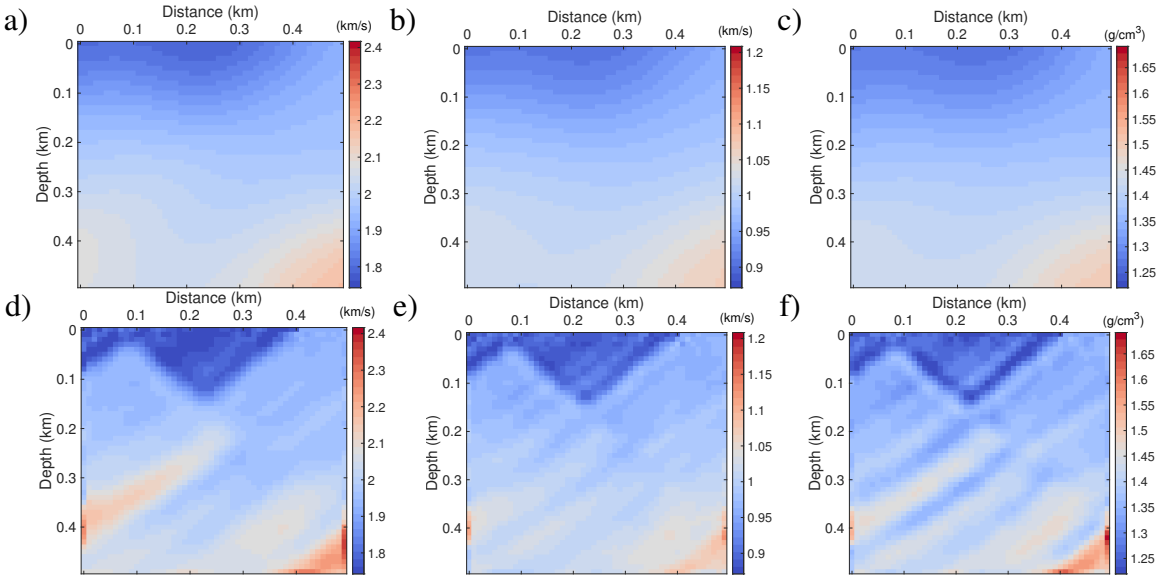

FIG. 2. The initial baseline models, (a) P-wave velocity, (b) S-wave velocity, and (c) density. The inverted baseline models, (d) P-wave velocity, (e) S-wave velocity, and (f) density.

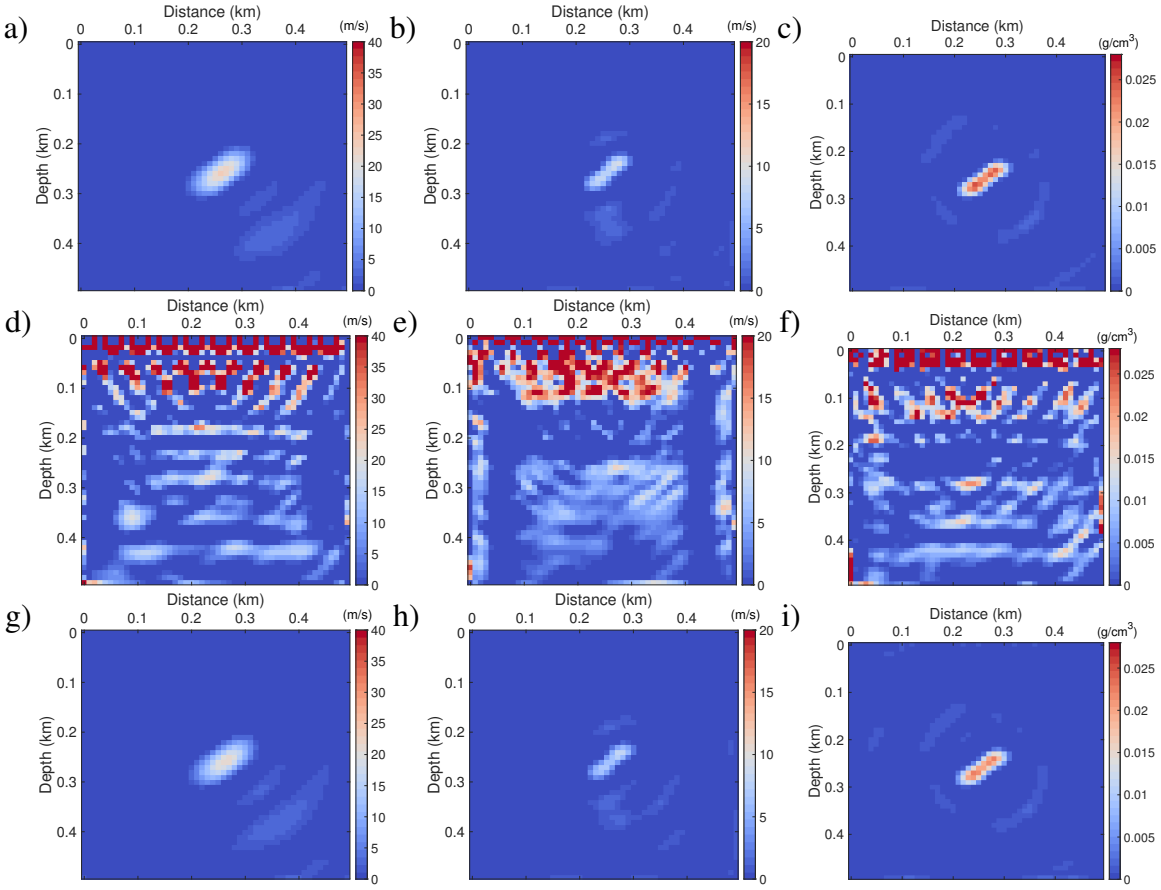

FIG. 3. The inverted time-lapse models of DDFWI in the case of baseline and monitoring wavelets are identical, (a) P-wave velocity, (b) S-wave velocity, and (c) density. The inverted time-lapse models of DDFWI in the case of baseline and monitoring wavelets are not identical, (d) P-wave velocity, (e) S-wave velocity, and (f) density. The inverted time-lapse models of DWDDFWI in the case of baseline and monitoring wavelets are not identical, (g) P-wave velocity, (h) S-wave velocity, and (i) density.

CONCLUSIONS

The DDFWI method demands good repeatability between baseline and monitor surveys, which is the most challenging for it. Especially, when source wavelets for baseline and monitor data sets are different, the results of DDFWI are seriously impacted, but DWDDFWI can handle this situation well. DWDDFWI works because the data difference caused by the wavelet difference is eliminated by the constructed common wavelet. DWDDFWI is developed based on the convolution relationship between the shot gather and Green's function. Our work has shown that the DWDDFWI works well for EFWI. The DWDDFWI for EFWI in the case of the baseline and monitoring data wavelets are different can provide the results as good as that provided by DDFWI in the case of the baseline and monitoring data wavelets are identical.

ACKNOWLEDGEMENTS

We thank the sponsors of CREWES for continued support. This work was funded by CREWES industrial sponsors, NSERC (Natural Science and Engineering Research Council

of Canada) through the grants CRDPJ 461179-13 and CRDPJ 543578-19. Partial funding also came from the Canada First Research Excellence Fund.

REFERENCES

Asnaashari, A., Brossier, R., Garambois, S., Audebert, F., Thore, P., and Virieux, J., 2011, Sensitivity analysis of time-lapse images obtained by differential waveform inversion with respect to reference model, *in* SEG Technical Program Expanded Abstracts 2011, Society of Exploration Geophysicists, 2482–2486.

Asnaashari, A., Brossier, R., Garambois, S., Audebert, F., Thore, P., and Virieux, J., 2014, Time-lapse seismic imaging using regularized full-waveform inversion with a prior model: which strategy?: Geophysical prospecting, **63**, No. 1, 78–98.

Brossier, R., Operto, S., and Virieux, J., 2009, Seismic imaging of complex onshore structures by 2d elastic frequency-domain full-waveform inversion: Geophysics, **74**, No. 6, WCC105–WCC118.

Denli, H., and Huang, L., 2009, Double-difference elastic waveform tomography in the time domain, *in* SEG Technical Program Expanded Abstracts 2009, Society of Exploration Geophysicists, 2302–2306.

Fu, X., Romahn, S., and Innanen, K., 2020, Double-wavelet double-difference time-lapse waveform inversion, *in* SEG Technical Program Expanded Abstracts 2020, Society of Exploration Geophysicists, 3764–3767.

Hicks, G. J., 2002, Arbitrary source and receiver positioning in finite-difference schemes using kaiser windowed sinc functions: Geophysics, **67**, No. 1, 156–165.

Lailly, P., Bednar, J. et al., 1983, The seismic inverse problem as a sequence of before stack migrations: Conference on Inverse Scattering, Theory and Application, Society for Industrial and Applied Mathematics, Expanded Abstracts, 206–220.

Maharramov, M., and Biondi, B., 2014, Joint full-waveform inversion of time-lapse seismic data sets, *in* SEG Technical Program Expanded Abstracts 2014, Society of Exploration Geophysicists, 954–959.

Oldenborger, G. A., Routh, P. S., and Knoll, M. D., 2007, Model reliability for 3d electrical resistivity tomography: Application of the volume of investigation index to a time-lapse monitoring experiment: Geophysics, **72**, No. 4, F167–F175.

Onishi, K., Ueyama, T., Matsuoka, T., Nobuoka, D., Saito, H., Azuma, H., and Xue, Z., 2009, Application of crosswell seismic tomography using difference analysis with data normalization to monitor co2 flooding in an aquifer: International Journal of Greenhouse Gas Control, **3**, No. 3, 311–321.

Pratt, R. G., 1990, Frequency-domain elastic wave modeling by finite differences; a tool for crosshole seismic imaging: Geophysics, **55**, No. 5, 626–632.

Raknes, E. B., and Arntsen, B., 2014, Time-lapse full-waveform inversion of limited-offset seismic data using a local migration regularization: Geophysics, **79**, No. 3, WA117–WA128.

Raknes, E. B., Weibull, W., and Arntsen, B., 2013, Time-lapse full waveform inversion: Synthetic and real data examples, *in* SEG Technical Program Expanded Abstracts 2013, Society of Exploration Geophysicists, 944–948.

Routh, P., Palacharla, G., Chikichev, I., and Lazaratos, S., 2012, Full wavefield inversion of time-lapse data for improved imaging and reservoir characterization, *in* SEG Technical Program Expanded Abstracts 2012, Society of Exploration Geophysicists, 1–6.

Routh, P. S., and Anno, P. D., 2008, Time-lapse noise characterization by inversion, *in* SEG Technical Program Expanded Abstracts 2008, Society of Exploration Geophysicists, 3143–3147.

Tarantola, A., 1984, Inversion of seismic reflection data in the acoustic approximation: Geophysics, **49**, No. 8, 1259–1266.

Virieux, J., and Operto, S., 2009, An overview of full-waveform inversion in exploration geophysics: Geophysics, **74**, No. 6, WCC1–WCC26.

Watanabe, T., Shimizu, S., Asakawa, E., and Matsuoka, T., 2004, Differential waveform tomography for time-lapse crosswell seismic data with application to gas hydrate production monitoring, *in* SEG Technical Program Expanded Abstracts 2004, Society of Exploration Geophysicists, 2323–2326.

Yang, D., Liu, F., Morton, S., Malcolm, A., and Fehler, M., 2016, Time-lapse full-waveform inversion with ocean-bottom-cable data: Application on valhall field: Geophysics, **81**, No. 4, R225–R235.

Yang, D., Meadows, M., Inderwiesen, P., Landa, J., Malcolm, A., and Fehler, M., 2015, Double-difference waveform inversion: Feasibility and robustness study with pressure data: Geophysics, **80**, No. 6, M129–M141.

Zheng, Y., Barton, P., and Singh, S., 2011, Strategies for elastic full waveform inversion of time-lapse ocean bottom cable (obc) seismic data, *in* SEG Technical Program Expanded Abstracts 2011, Society of Exploration Geophysicists, 4195–4200.